Journal of Power Sources 188 (2009) 64–74

Contents lists available at ScienceDirect

Journal of Power Sources

journal homepage: www.elsevier.com/locate/jpowsour

Tuning the performance of direct methanol fuel cell membranes by embedding multifunctional inorganic submicrospheres into polymer matrix

Jingtao Wang [a], Han Zhang [b], Zhongyi Jiang [a,*], Xinlin Yang [b,**], Lulu Xiao [a]

[a] Key Laboratory for Green Chemical Technology, School of Chemical Engineering and Technology, Tianjin University, Tianjin 300072, China
[b] Key Laboratory of Functional Polymer Materials, Ministry of Education, Institute of Polymer Chemistry, Nankai University, Tianjin 300071, China

ARTICLE INFO

Article history:
Received 12 October 2008
Received in revised form
14 November 2008
Accepted 17 November 2008
Available online 3 December 2008

Keywords:
Chitosan
Multifunctional inorganic submicrospheres
Hybrid membrane
Free volume characteristics
Proton acceptor/donor capability

ABSTRACT

A series of surface functionalized silica submicrospheres by distillation–precipitation polymerization were embedded into chitosan (CS) matrix to fabricate the hybrid membranes for direct methanol fuel cell (DMFC). SEM characterization indicated that the submicrospheres could disperse homogenously within the CS matrix via tuning the polymer/particle and particle/particle interfacial interactions. The incorporation of sulfonated silica and carboxylated silica led to the reduced fractional free volume (*FFV*), whereas the incorporation of quaternary aminated silica resulted in increased *FFV* in the hybrid membranes, which was confirmed by the free volume characteristics analysis using positron annihilation lifetime spectroscopy (PALS). The correlation between methanol crossover and *FFV* was established: the hybrid membranes with lower *FFV* displayed higher methanol resistance. Meanwhile, the correlation between the proton acceptor/donor capability and proton conductivity in the hybrid membranes was established. Compared with sulfonated silica and quaternary aminated silica, carboxylated silica possessed the optimum matching in proton acceptor and donor capabilities. Therefore, the membrane embedded with carboxylated silica displayed the highest proton conductivity. In particular, embedding carboxylated silica simultaneously reduced the methanol permeability by 63% and increased the proton conductivity by 40% in comparison with pure CS membrane.

1. Introduction

Organic–inorganic hybrid membranes have triggered considerable interest in virtue of their extraordinary properties arising from the synergism of the properties between the two different building materials [1–4]. Hybrid proton exchange membranes (PEMs) comprising bulk polymer embedded by inorganic additives, such as SiO_2 [5,6], ZrO_2 [7], TiO_2 [8], zeolite [9,10], zirconium phosphate [11], montmorillonite [12] and clinoptildite [13], have recently been proposed as promising electrolytes for direct methanol fuel cell (DMFC) application.

Methanol crossover from anode to cathode, which drastically reduces the DMFC performance due to the mixed potential effect and catalyst poisoning, critically restricts its practical application [14]. Tremendous efforts have been devoted to suppressing methanol crossover by embedding inorganic fillers into polymer matrix. To sum up, embedding nonporous fillers (e.g. silica and zirconia) or porous fillers (e.g. zeolite) within bulk polymer both introduced a tortuous diffusion path for methanol molecules and consequently decreased the methanol crossover [9,15,16]; however, embedding porous fillers increased the probability of methanol molecules (kinetic radius 0.19 nm) diffusion directly through the pores (e.g. mordenite pore size 0.7 nm) [9,15]. Compared to sheet fillers (e.g. montmorillonite) and tubular fillers (e.g. carbon nanotube), spherical fillers (e.g. silica) displayed most significant effects in inhibiting methanol crossover owing to both their sufficient contact with the polymer chain and their best dispersion behavior [17–19]. Among nano-sized, submicron-sized, and micron-sized fillers, submicron-sized fillers (diameter between 100 nm and 1.0 μm) exhibited the optimum methanol-barrier property considering the fact that excessively small or big fillers would generate agglomeration or sedimentation during membrane fabrication which often caused non-ideal defects within the membranes [17,20,21]. It should be noted that the chemical modification of inorganic fillers is often employed to tune the interaction between inorganic fillers and polymer [4,20]. The transport of methanol within DMFC membrane can be described by solution-diffusion mechanism, in which the process is dominated by the diffusivity of the methanol in most cases [18,22,23]. For the dense hybrid membrane, the diffusion channel is often provided by the free volume cavities, which exist as either static voids due to inefficient chain packing or transient gaps during the thermal induced chain

* Corresponding author. Tel.: +86 22 27892143; fax: +86 22 27892143.
** Corresponding author. Tel: +86 22 23502023; fax: +86 22 23503510.
E-mail addresses: zhyjiang@tju.edu.cn (Z. Jiang), xlyang88@nankai.edu.cn (X. Yang).

0378-7753/$ – see front matter © 2008 Elsevier B.V. All rights reserved.
doi:10.1016/j.jpowsour.2008.11.109

rearrangement [24–26]. Therefore, it is important and useful to elucidate the correlation between free volume characteristics and methanol permeability.

Proton conductivity is another key parameter for proton exchange membrane which directly affects operational fuel cell voltage and current output of a DMFC [27,28]. Significant contributions have been devoted to improving proton conductivity of the DMFC membranes through appropriate chemical modification. Previously, immersing the as-prepared membrane into acid solution constituted a facile approach. These acid-doped membranes bearing sufficient amount of acid groups displayed desirable proton conductivity (in range of 10^{-2} to 10^{-1} S cm^{-1}) due to the high degree of self-dissociation of the acid groups, as well as high water uptake (resulting from the enhanced hydrophilicity) of the membranes [29,30]. However, the excessive water swelling and acid leaching from the membrane because of the cleavage of ionic bonds between acid groups and polymer chains limited their practical application [5,6,31]. Modification of the polymer matrix prior to membrane fabrication becomes more and more popular recently, sulfonation has been demonstrated as the most commonly utilized approach for the chemical especially for aromatic polymers (e.g. poly(styrene), poly(arylene ether)s, and poly(imide)s) because of their high activity in electrophilic substitution reaction [32,33]. A high sulfonation level corresponded to high proton conductivity (between 10^{-3} and 10^{-1} S cm^{-1}) [34]. However, a high sulfonation level often induced high methanol crossover due to the excessive water swelling, as well as low thermal and chemical stabilities [29,35]. Compared with sulfonic acid group, phosphoric acid group exhibited lower average zero point energy and higher water binding energy [36], therefore, phosphoric acid-bearing membranes had been regarded as a promising alternative in PEM [32,37]. These membranes displayed high proton conductivity (between 10^{-2} and 10^{-1} S cm^{-1}) due to their low proton migration barrier and high water retention properties under certain phosphorylation level. However, the rather limited synthesis procedures available and excessive water swelling impeded their wide utilization in DMFC [31,32]. In comparison, chemical modification of inorganic fillers by sulfonic acid (sulfonated montmorillonite), phosphoric acid (zirconium phosphate) and heteropolyacid (zirconia phosphotungstic acid) has gained increasing attention as an effective, generic, facile approach to introduce acid groups, which rendered additional proton-conducting pathway and retained more water molecules [38–40]. The hybrid membranes with acid-functionalized fillers exhibited desirable thermal and mechanical stabilities, as well as high proton conductivity. Unfortunately, majority studies focused on the proton donor property of the acid groups while quite few studies focused on the proton acceptor property of the acid groups. In recent studies, Narayanan et al. observed that the activation energy (energy barrier) for proton migration of weak base/weak acid composite (0.03 eV) was significantly lower than that of weak base/strong acid composite (0.31 eV) at 160–180 °C [41]. Kreuer et al. systematically examined the proton diffusion and conductivity in various of basic and acidic compounds, and found that the compounds with moderate proton donor and acceptor properties produced higher proton mobility [42,43]. It can be naturally conjectured that the PEM with moderate and well-matched proton donor and acceptor capabilities will display high proton conductivity. Therefore, it is important and useful to elucidate the correlation between proton acceptor/donor capability and proton conductivity. Theoretically and technologically, appropriate functionalization of inorganic filler may be served as a facile approach to simultaneously tailor the proton acceptor capability and donor capability of the hybrid PEM.

In this study, a series of hybrid membranes for DMFC were prepared by embedding silica–polymer core-shell submicrospheres with different functional groups into chitosan (CS) matrix through a facile solution-casting method. The main objective of this study was to fabricate high performance hybrid membrane with low methanol crossover and high proton conductivity through tuning free volume characteristics and proton acceptor/donor capability of the membrane. The properties of the prepared membrane were extensively evaluated, including water uptake, methanol permeability, proton conductive, chemical and physical properties etc. Hopefully, some useful guidelines concerning the rational design and preparation of inorganic fillers in the hybrid membranes could be derived.

2. Experimental

2.1. Materials

Tetraethyl orthosilicate ($Si(OEt)_4$, TEOS) and ethyleneglycol dimethacrylate (EGDMA) were purchased from Aldrich and Alfa Aesar respectively, and used without any further purification. 4-Vinylpyridine (VPy) was available from Acros and distilled under vacuum. Divinylbenzene (DVB, 80% divinylbenzene isomers) was supplied as technical grade by Shengli Chemical Technical Faculty, Shandong, China, and was washed with 5% aqueous sodium hydroxide and water, then dried over anhydrous magnesium sulfate prior to use. 3-(Methacryloxy)propyltrimethoxysilan (MPS) was supplied by Aldrich and distilled under vacuum. 2,2′-Azobisisobutyronitrile (AIBN), methacrylic acid (MAA), benzyl chloride (BCL) and acetonitrile were purchased from Tianjin. MAA was purified by vacuum distillation before use. CS with a degree of deacetylation of 91% was purchased from Golden-Shell Biochemical Co. (Zhejiang, China) and used as received. All the other reagents were commercially available as analytical grade and used without any further purification. De-ionized water was used in all experiments.

2.2. Preparation of monodisperse core-shell silica–polymer submicrospheres with various functional groups on the shell-layer by distillation–precipitation polymerization

Silica submicrospheres were prepared according to classical the Stöber method: 12 mL of TEOS was added to the mixture of 200 mL ethanol, 20 mL water and 15 mL aqueous solution of 25% ammonium with vigorous stirring at room temperature. Then excess MPS (1.0 g, 4.0 mmol) was introduced into 20 mL of the silica mixture under stirring. After being stirred for 48 h at room temperature, the mixture of alcosol silica particles and MPS were purified by three cycles of centrifugation, decantation, and re-suspended in ethanol with ultrasonic-bathing. The MPS-modified silica particles were dried in a vacuum oven at 50 °C till constant weight.

The silica–polymer core-shell submicrospheres with various functional groups on the shell-layer in the presence of MPS-modified silica particles as the seeds were prepared by distillation–precipitation polymerization [44]. A typical procedure for the synthesis of silica–polymer is as follows: MPS-modified silica (0.10 g), DVB (0.40 mL, 0.37 g), and AIBN (0.008 g) were dissolved in 40 mL of acetonitrile in a dried 50 mL two-necked flask, attached with a fraction acting column, Liebig condenser, and a receiver. The mixture was heated by a heating mantle from ambient temperature till boiling state within 15 min and then the solvent was distilled off from the reacting system. The reaction was stopped until 20 mL of acetonitrile was distilled out from the reaction system within 70 min. After being purified and dried, the resultant core-shell silica-poly(divinylbenzene) submicrospheres were sulfonated by concentrated sulfuric acid (94%) at 40 °C for 4 h according to the procedure in the literature [45], then monodisperse core-shell silica submicrospheres with sulfonic groups on the shell-layer (silica-SO_3H) were obtained.

Core-shell silica/poly(ethyleneglycol dimethaccrylate-co-methacrylic acid) (silica-CO_2H) [46] with carboxylic acid group and silica/poly(ethyleneglycol dimethaccrylate-co-vinyl pyridine) (silica-Py) [47] with pyridyl group on the shell-layer were prepared according to the literature by distillation precipitation copolymerization of EGDMA with crosslinking degree as 0.50 and the functional comonomers MAA and VPy, respectively. Cationic silica-poly(EGDMA-co-vinylpyridinium benzyl chloride) (silica-QPy) was prepared by the pyridinium modification of pyridyl group of silica-Py with BCL as quaternary aminating agent.

2.3. Membrane preparation

CS (1.5 g) was dissolved in 40 mL of 2 wt% acetic acid aqueous solution under stirring at 80 °C. Simultaneously, silica (0.3 g, 20 wt% corresponding to CS) was dispersed into 35 mL of 2 wt% acetic acid aqueous solution with ultrasonic treatment for 30 min. These two parts of solution were then mixed and stirred vigorously at 80 °C for another 2 h. After degasification, the resulting homogenous solution was cast onto a clear glass plate and dried at 25 °C. The membrane was afterwards immersed and cross-linked in 2 M H_2SO_4 for 24 h and then extensively rinsed with de-ionized water to remove residual H_2SO_4. Finally the membrane (CS/silica) was dried under vacuum at 25 °C for 24 h. Pure chitosan membrane and silica-SO_3H, silica-Py, silica-QPy and silica-CO_2H filled membranes were prepared and designated, respectively as CS, CS/silica-SO_3H, CS/silica-Py, CS/silica-QPy and CS/silica-CO_2H. It should be pointed that membrane thickness was in range of 50–60 μm.

2.4. Characterization

The size and morphology of silica and silica–polymer submicrospheres were characterized by transmission electron microscopy (TEM, Tecnai G2 20 S-TWIN). The morphology of the membranes was observed by scanning electron microscopy (SEM, Philips XL 30 ESEM). Membrane samples were freeze-fractured in liquid nitrogen and then sputtered with gold prior to measurement.

Fourier transform infrared spectra (FTIR, 4000–400 cm^{-1}) of the submicrospheres and the membrane were recorded on a Nicolet-740 50X instrument.

The crystalline structures of the membranes were investigated with a RigakuD/max2500v/Pc X-ray diffractometer (XRD, CuK 40 kV, 200 mV, 2° min^{-1}) in the range of 3–45°. The peak position and its area were extracted with MDIjade5 software.

The thermogravimetric analysis (TGA-50, SHIMDZU) data of the membranes were obtained from 30 to 350 °C using a heating rate of 10 °C min^{-1} at air atmosphere.

Positron annihilation lifetime spectroscopy (PALS) experiment was performed by using an EG&GORTEC fast–fast coincidence system (resolution 181 ps) at room temperature. The resource of ^{22}Na (5×10^5 Bq) was sandwiched between two pieces of sample, each with an overall thickness of about 1 mm. The integral statistics for each spectrum was more than 2×10^6 coincidences. The spectrum was analyzed using LT-v9 program.

2.5. Water uptake, swelling, and ion exchange capacity (IEC)

The water uptake of the membranes was determined as following. The dry membrane was weighed (W_{dry}) and immersed in de-ionized water for 24 h at room temperature. Then the membrane was re-weighed (W_{wet}) quickly after removing the surface water. The surface swelling was determined in a similar manner, by soaking the pre-measured membrane (A_{dry}) in de-ionized water for 24 h, then re-measuring to obtain the wetted membrane area (A_{wet}). The final values of water uptake and swelling were the average of the three measurements with an error within ±5.0% and calculated by Eqs. (1) and (2), respectively:

$$\text{Water uptake } (\%) = \frac{W_{wet} - W_{dry}}{W_{dry}} \times 100 \quad (1)$$

$$\text{Swelling } (\%) = \frac{A_{wet} - A_{dry}}{A_{dry}} \times 100 \quad (2)$$

IEC values of the submicrosphere and membrane were determined by titration method. The pre-weighted sample in H^+ form was immersed in 2 M NaCl solution for 24 h to replace the H^+ by Na^+ completely. The remaining solution was then titrated with a 0.01 M NaOH solution using phenolphthalein as indicator. The *IEC* value was calculated by Eq. (3):

$$IEC \ (\text{mmol g}^{-1}) = \frac{0.01 \times 1000 \times V_{NaOH}}{W_d} \quad (3)$$

where V_{NaOH} is the volume of NaOH solution consumed in the titration and W_d is the weight of the dry sample. The measurements were carried out with an accuracy of 0.001 mmol g^{-1}.

2.6. Methanol permeability

The methanol permeability was measured with a glass diffusion cell as described in the literature [15], which consisted of two compartments with identical volume separated by the membrane sheet. The membrane was hydrated in de-ionized water for 24 h before being clamped tightly between the two compartments, one of which was initially filled with water and the other filled with methanol solution (2 M or 12 M). The methanol concentration in the receipt compartment was determined using a gas chromatography (Agilent 6820) equipped with a TCD detector and a DB624 column. The methanol permeability (P, $cm^2\ s^{-1}$) was calculated from Eq. (4):

$$P = S\frac{V_B l}{AC_{A0}} \quad (4)$$

where S is the slope of the straight line of concentration vs. time, V_B is the volume of the receipt compartment, l, A, and C_{A0} are the membrane thickness, effective membrane area, and feed concentration, respectively. The measurement error was within ±4.0%.

2.7. Proton conductivity

The proton conductivity of the membranes in the transverse direction was measured in two-point-probe conductivity cells by the ac impedance spectroscopy method over a frequency range of 1–10^6 Hz with oscillating voltage of 10 mV, using a frequency response analyzer (FRA, Autolab PGSTST20) at 20 ± 1 °C. All the membrane samples were immersed in 0.2 M H_2SO_4 for 24 h prior to measurement in order to eliminate the contact resistance between 316 L electrode and membrane surface, which was similar to the treatment adopted in the literature [14,15]. The proton conductivity (σ, S cm^{-1}) of the sample in transverse direction was calculated by Eq. (5):

$$\sigma = \frac{l}{AR} \quad (5)$$

where l and A are distance between the electrodes and membrane area, respectively, and R is the membrane resistance derived from the low intersect of the high frequency semicircle on a complex impedance plane with Re (z) axis.

3. Results and discussion

3.1. Characterization of silica and silica–polymer submicrospheres with various functional groups

Inorganic-polymer hybrid submicrospheres combine the advantages of both inorganic and organic materials such as mechanical strength modulus, flexibility, and various functional groups. Scheme 1 illustrated the synthetic procedure of bare silica, MPS-modified silica, and core-shell silica–polymer hybrid submicrospheres with various functional groups on the shell-layer.

The monodisperse MPS-silica inorganic cores were prepared by the hydrolysis of siloxane TEOS via a typical sol–gel process with the subsequent coating of MPS to incorporate the reactive vinyl groups on the surface as the first-stage reaction in the present work. The formation of polymer shell-layer was achieved by the second-stage distillation precipitation polymerization with the aid of the reactive vinyl groups on the surface of MPS-modified silica seeds to capture the newly formed oligomers and monomers [44]. DVB and EGDMA were used as crosslinkers during the polymerization, in which DVB, MAA and VPy were utilized to introduce the phenyl, carboxylic acid, and pyridyl group, respectively. Fig. 1 showed the typical TEM micrographs of silica and representative core-shell submicrospheres (silica-CO_2H), in which the particles with spherical shape were clearly observed.

The diameters, shell thickness and *IEC* values of the silica, core-shell silica–polymer submicrospheres were summarized in Table 1. The results indicated that the diameters of the resultant core-shell hybrid particles were significantly increased from 400 nm of silica core to 418–436 nm of the silica–polymer core-shell particles, which implied that 9–18 nm of the polymer shell with different functional groups were successfully coated onto the silica seeds via the second-stage distillation precipitation polymerization. The different thicknesses of the polymer shell for the core-shell hybrid submicrospheres were afforded due to the different reactivity of the comonomers.

Table 1
The diameter, shell thickness, and *IEC* values of silica and silica–polymer materials.

Entry	1	2	3	4	5
Submicrosphere	Silica	Silica-Py	Silica-QPy	Silica-CO_2H	Silica-SO_3H
Diameter (nm)	400	418	418	422	436
Shell thickness (nm)	0	9	9	11	18
IEC (mmol g^{-1})		0.039	0.028	0.045	0.056

The surface modification of the silica seeds via the second-stage polymerization to incorporate the different functional groups on the polymer shell-layer was confirmed further by FTIR spectra as shown in Fig. 2. For the silica core particles, the FTIR spectrum in Fig. 2a had a strong peak at 1140 cm^{-1} and a middle peak at 802 cm^{-1} corresponding to the symmetric and asymmetric stretching vibration of Si—O—Si together with a middle peak at 954 cm^{-1} assigning to the stretching vibration of hydroxyl group. The FTIR spectrum, in Fig. 2b of silica-CO_2H possessed the peaks at 1449 cm^{-1}, which was attributed to the bending of COO—H and 1705 cm^{-1} corresponding to the carbonyl unit of the carboxylic acid group [34,48]. The characteristic peaks of the sulfonic group (1420–1310 cm^{-1} and 1235–1145 cm^{-1}), respectively, attributing to the asymmetric and symmetric O=S=O stretching vibration bands could not be discriminated because they were overlapped by the strong and broad peak of silica at 1104 cm^{-1}. The FTIR spectrum in Fig. 2d had weak but obvious peaks at 1550 and 1660 cm^{-1} corresponding to the typical vibration of the pyridyl group [49]. In the FTIR spectrum of silica-QPy (Fig. 2e), a new peak appeared at 1637 cm^{-1} attributing to the stretching vibration of the pyridinium reaction of the pyridinium group. All these results demonstrated

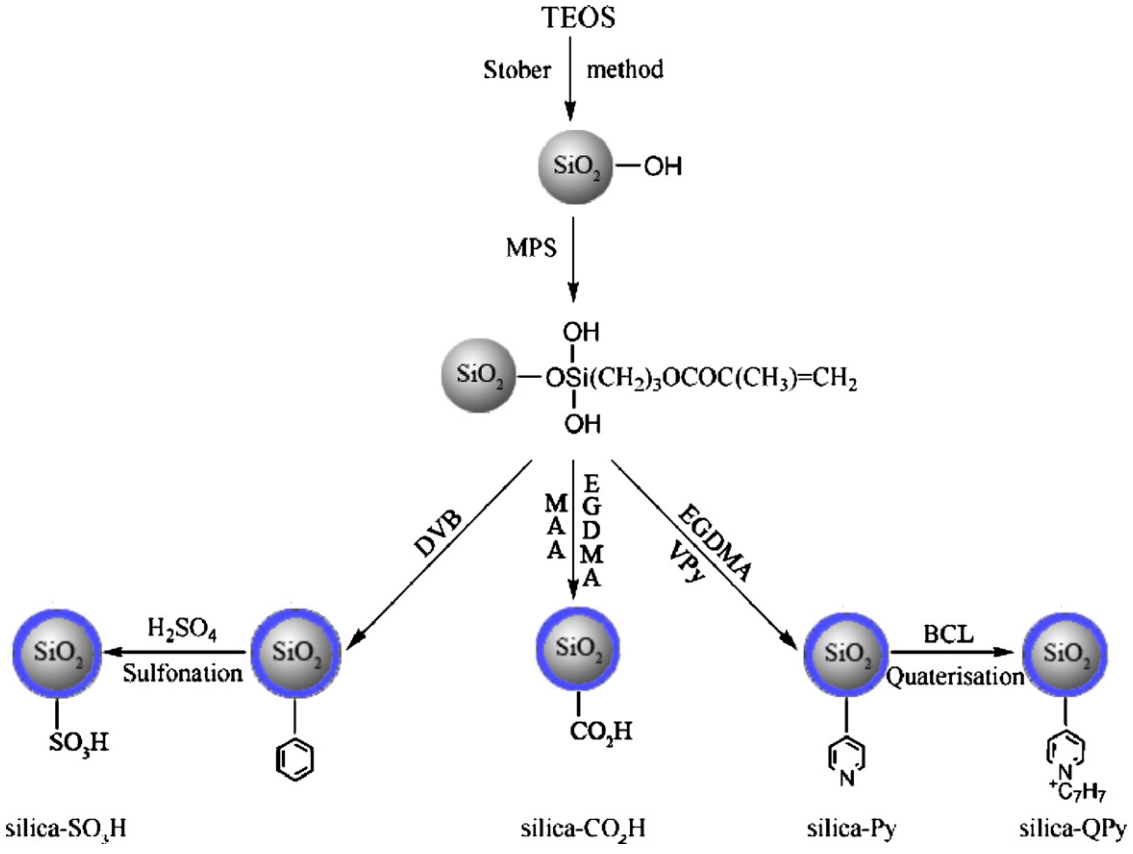

Scheme 1. Preparation of silica and silica–polymer core-shell submicrospheres and the corresponding chemical reactions.

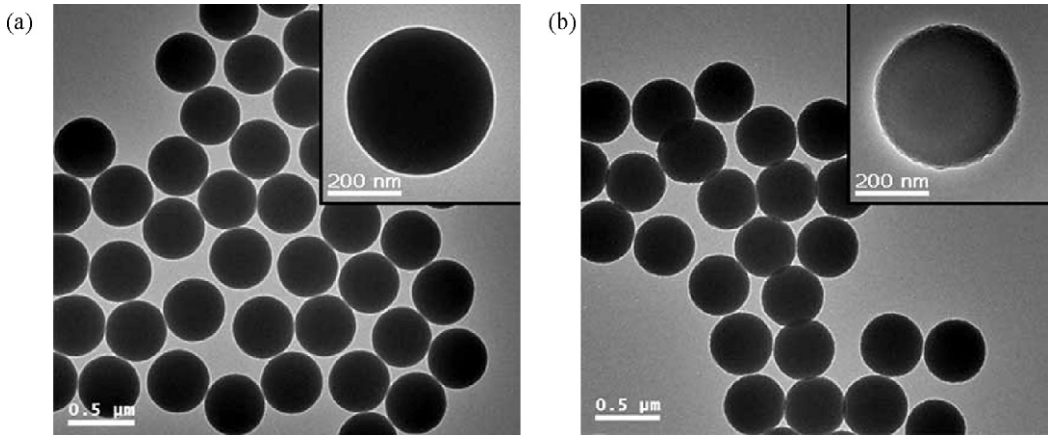

Fig. 1. Micrograph of submicrospheres: TEM micrograph of (a) silica and (b) silica-CO_2H submicrospheres.

that the polymer shell-layer was successfully prepared by the second-stage distillation precipitation polymerization and via the subsequent surface modification, which allowed the possibility to tailor the performance of DMFC membranes by embedding multi-functional functionalized inorganic submicrospheres into polymer matrix.

3.2. Elucidation the homogeneous dispersion of submicrospheres in the membrane

During the membrane fabrication, homogeneous dispersion of fillers would produce more effective polymer/particle interfacial area, and offer more possibility of surface-induced tailoring of the morphology, hence potentially improving the membrane performance, whereas sedimentation and agglomeration would cause micro-phase separation and non-selective voids in the membrane [4,21].

The dispersion of fillers within the membranes was probed by SEM as shown in Fig. 3. Since the inorganic filler with the size smaller than 500 nm possessed relatively low sedimentation rate [50], in the present study, silica and functionalized silica–polymer submicrospheres with an average diameter in the range of 400–436 nm were utilized. To tailor the membrane performance effectively and elucidate the influence of the functional groups on the dispersion of the submicrospheres, 20 wt% fillers corresponding to CS were embedded into polymer matrix for each hybrid membrane. Fig. 3b indicated that silica particles agglomerated and moved to the membrane surface driven by the surface tension during the membrane preparation. This was mainly attributed to the poor interfacial compatibility between silica and bulk polymer, and similar observation was reported in the literature [17,51]. After surface modification, due to the presence of the hydrophilic polymeric shell-layer, the interfacial compatibility was improved, which would decrease the surface tension and consequently depress the migration. Therefore, the dispersion effect of the functionalized submicrospheres was obviously improved (Fig. 3c–f) compared to silica embedded membrane. On the other hand, it was generally known that when the particle diameter was in range of 10^{-7} m, particles were mainly in Brownian motion within the casting suspension. Accordingly, when the particles collided with each other in the casting suspension, particles would agglomerate driven by the hydrogen-bonding interactions between the polar groups (—OH and —NH_2) of the particles, which could be seen clearly in SEM images (Fig. 3b and c). The morphologies of CS/silica-QPy (Fig. 3d), CS/silica-CO_2H (Fig. 3e), and CS/silica-SO_3H (Fig. 3f) indicated the homogeneous dispersion of the functionalized silica fillers in the membrane. Such phenomenon was reasonably attributed to the fact that these three kinds of filler had electrostatic charge within the casting suspension, which would result in strong electrostatic repulsive force between the particles during their collision. In these cases, the particle agglomeration was effectively depressed. The SEM results implied that the submicrospheres could disperse homogeneously within polymer matrix through appropriate surface modification, which ensured the effective manipulation of the membrane properties for DMFC.

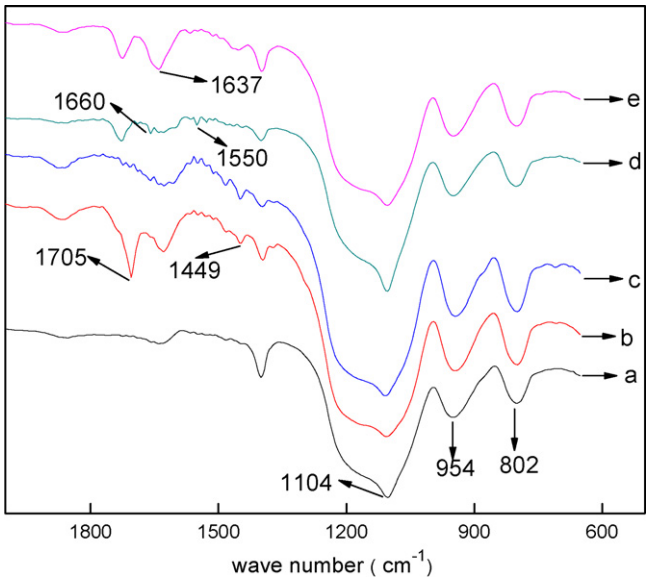

Fig. 2. FTIR spectra of the submicrospheres: (a) silica; (b) silica-CO_2H; (c) silica-SO_3H; (d) silica-Py; (e) silica-QPy.

3.3. Characterization of the membranes

The influence of the submicrospheres on physicochemical properties of the hybrid membranes were investigated using FTIR, TGA, and XRD, and shown in Figs. 4–6, respectively. FTIR spectra have been utilized to gain a better understanding of the interfacial interaction between fillers and CS. The characteristic peaks of CS in FTIR spectra (Fig. 4a), viz., the hydroxyl and amide I and II groups were located at 3358 cm^{-1} and 1648, 1565 cm^{-1} respectively [48]. According to Fig. 4, the intensity of the characteristic peaks of hybrid membrane varied with the functional group of the fillers. As shown in Fig. 4c and d, the intensity of these three peaks in CS/silica-Py and CS/silica became weak, which should be originated from the

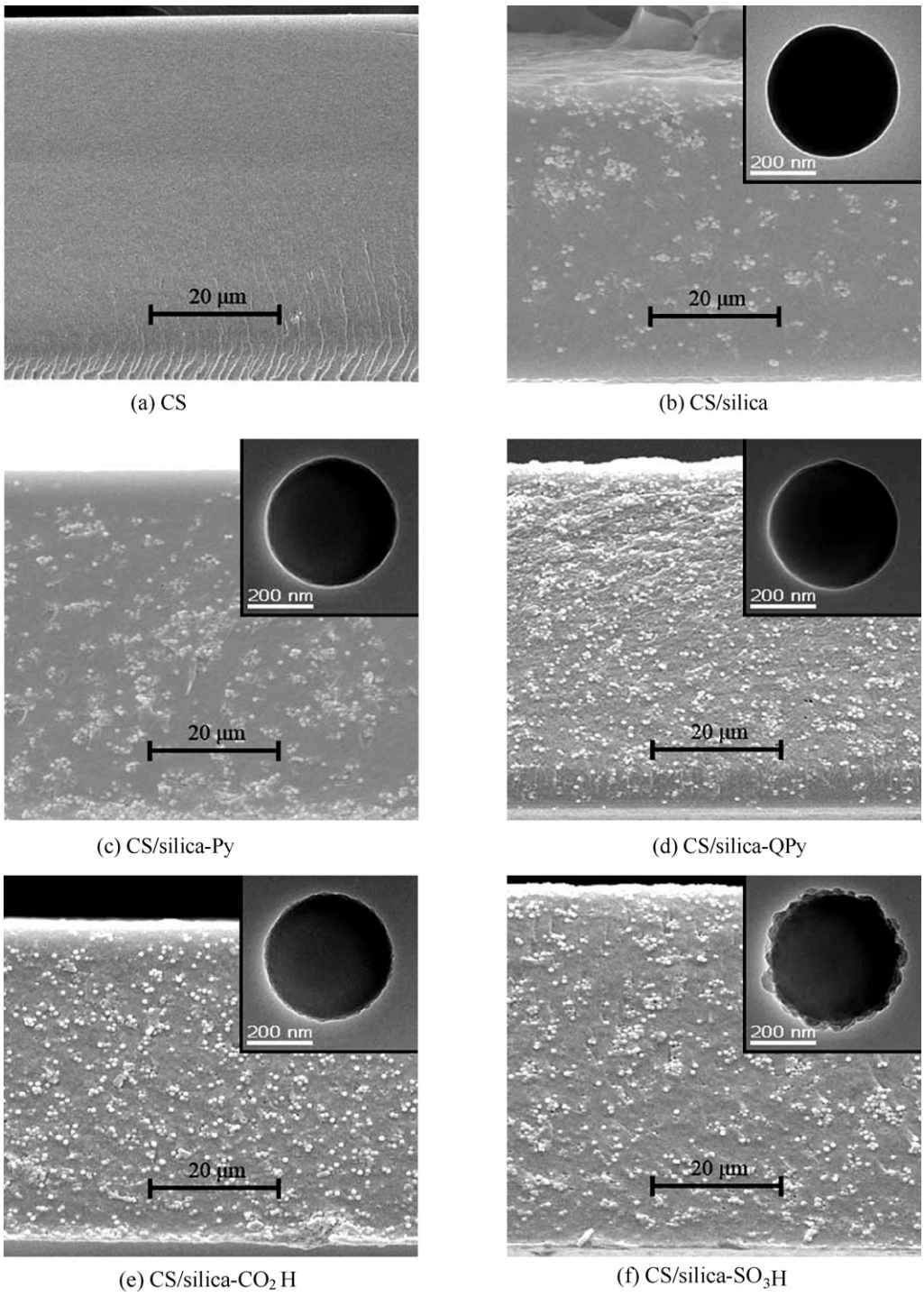

Fig. 3. SEM images of the cross section of the membranes: (a) CS; (b) CS/silica; (c) CS/silica-Py; (d) CS/silica-QPy; (e) CS/silica-CO_2H; (f) CS/silica-SO_3H.

hydrogen-bonding interactions between CS chains and particles bearing hydrophilic groups. As reported by literatures, the amino groups in CS would be partially protonated to $-H_3N^+$ in acid solution during membrane preparation [48,52]. Therefore, the presence of cations in silica-QPy would cause electrostatic repulsive force between the particles and CS chains, which inhibited the formation of hydrogen bonds between CS and the fillers. The intensity of the peak of CS/silica-QPy at 3358 cm^{-1} (Fig. 4b) was therefore a little stronger than that of CS/silica-Py. In contrast when incorporating silica-CO_2H or silica-SO_3H particles, strong and extensive electrostatic attractive force between —OH and $-NH_2$ of CS and $-CO_2$H or $-SO_3$H of particles was formed, which remarkably weakened the intensity of the characteristic peaks at 3358, 1648, and 1565 cm^{-1} (Fig. 4e and f).

TGA curves shown in Fig. 5 indicated that all membranes exhibited two major weight loss stages: the first weight loss region (50–100 °C) was attributed to the evaporation of adsorbed water; the second weight loss region (210–300 °C) was corresponded to the decomposition of CS chains, which agreed with the results in the literature [53]. According to TGA results, CS/silica-QPy (Fig. 5a) exhibited the lowest thermal stability among these membranes. Such phenomenon suggested that silica-QPy parti-

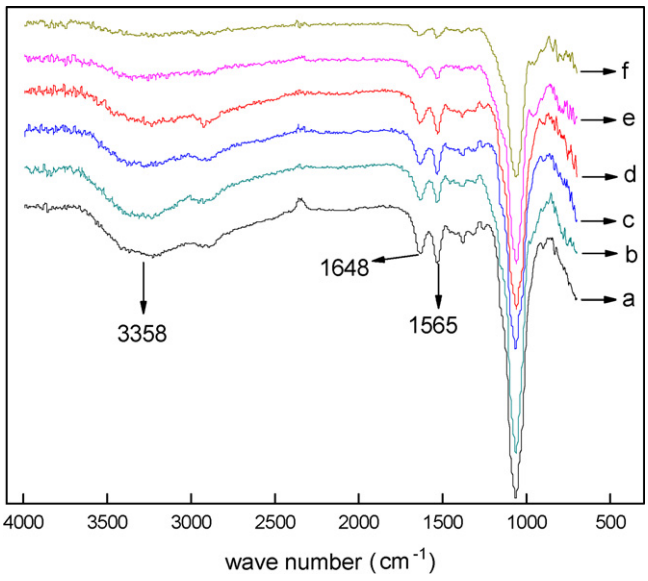

Fig. 4. FTIR spectra of the membranes: (a) CS; (b) CS/silica-QPy; (c) CS/silica-Py; (d) CS/silica; (e) CS/silica-CO_2H; (f) CS/silica-SO_3H.

cles would reduce the hydrogen bonds between CS chains and simultaneously engendered electrostatic repulsive force with CS chains, which could synergistically loose the chain packing and enhance the chain mobility. In comparison, when incorporating silica-Py or silica, the formation of hydrogen-bonding interactions between CS and fillers dramatically suppressed the decomposition of CS molecules, and resulted in enhancing thermal stability (Fig. 5c and d) compared to pure CS membrane. Furthermore, the thermal stability of CS/silica-CO_2H (Fig. 5e) and CS/silica-SO_3H (Fig. 5f) were significantly enhanced, which indicated that the mobility of CS chains was effectively inhibited due to the strong electrostatic attractive force between CS and functionalized silica particles. The TGA data implied that the thermal stability of the hybrid membranes, which was determined by the mobility of the polymer chains, could be tailored by the interfacial interactions between polymer and fillers: strong attractive force would enhance the stability whereas repulsive force would decrease the stability of the membrane.

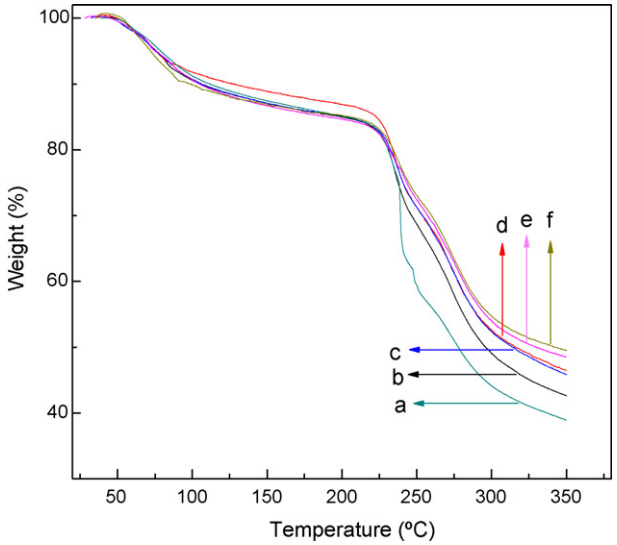

Fig. 5. TGA thermodiagram of CS and hybrid membranes: (a) CS/silica-QPy; (b) CS; (c) CS/silica-Py; (d) CS/silica; (e) CS/silica-CO_2H; (f) CS/silica-SO_3H.

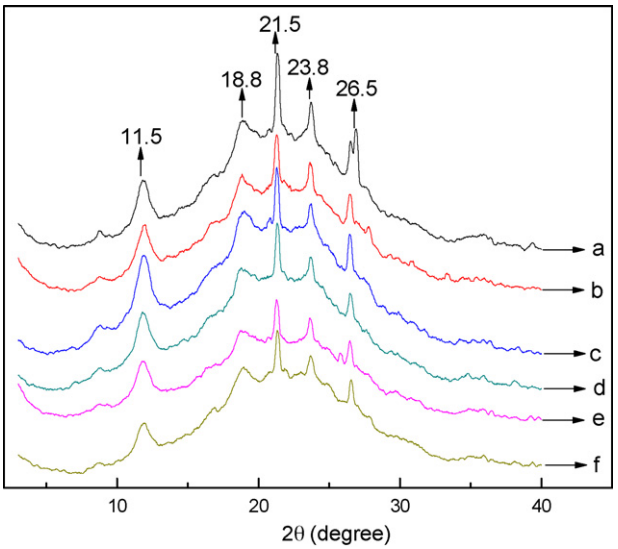

Fig. 6. XRD patterns of (a) CS, (b) CS/silica, (c) CS/silica-Py, (d) CS/silica-QPy, (e) CS/silica-CO_2H, and (f) CS/silica-SO_3H membranes.

The membranes were also subjected to XRD analyses to evaluate the influence of inorganic fillers on crystalline structures of CS. In agreement with the observation by Yuan et al. [53], the CS membrane (Fig. 6a) exhibited both of the two crystal peaks of I (11.5° and 18.8°) and II (21.5°, 23.8° and 26.5°) due to the semicrystalline character of CS. For hybrid membranes (Fig. 6b–f), the presence of inorganic fillers interfered the ordered packing of CS chains, destroying the crystalline domain by steric effects and/or interactions between CS and additives. Fig. 6b and c demonstrated that the presence of silica and silica-Py disrupted the ordered packing of CS chains by hydrogen-bonding interactions, and lowered the crystalline degree of CS. In comparison, the intensity of the characteristic peaks in CS/silica-CO_2H (Fig. 6e) and CS/silica-SO_3H (Fig. 6f) decreased remarkably due to the strong and extensive electrostatic interaction between CS and the particles, which significantly disrupted CS chain packing.

3.4. Free volume characteristics analysis and methanol permeability evaluation of the membrane

3.4.1. Free volume characteristics

Free volume characteristics, reflecting the mobility and packing of polymer chains, are reported as an effective direct datum for describing the morphology of the membrane [3,25,53]. Previous results demonstrated that the free volume of the polymer in the region directly contacting the particles was different from that of the bulk polymer, and the interfacial interaction might exert considerable influence on the interfacial morphology of hybrid membranes [25,54]. Since the transport properties of hybrid membrane are strongly dependent on the nanoscale morphology of the membrane, it is necessary to gain a deeper understanding of the effects of filler on the free volume characteristics of hybrid membrane.

PALS technique has been employed as a unique direct way to probe the free volume in dense membrane, and in this technique, assuming that o-Ps was localized in a spherical potential well surrounded by an electron layer of thickness Δr equal to 0.1656 nm, the radius of free volume cavity (r) is obtained from pick-off annihilation lifetime (τ) of o-Ps in the free volume elements [25,54,55] by a semi-empirical equation:

$$\tau = \frac{1}{2}\left[1 - \frac{\gamma}{\gamma + \Delta\gamma} + \left(\frac{1}{2\pi}\right)\sin\left(\frac{2\pi\gamma}{\gamma + \Delta\gamma}\right)\right]^{-1} \quad (6)$$

Table 2
Free volume parameters of CS and hybrid membranes.

Entry	Membrane	τ_3 (ns)	I_3 (%)	r_3 (nm)	V_f (nm^3)	*FFV* (%)
1	CS	1.90	13.15	0.276	0.088	1.154
2	CS/silica	1.87	14.07	0.273	0.085	1.196
3	CS/silica-Py	1.84	14.37	0.270	0.082	1.186
4	CS/silica-QPy	1.97	13.44	0.282	0.094	1.267
5	CS/silica-CO_2H	1.82	13.86	0.268	0.080	1.113
6	CS/silica-SO_3H	1.80	13.62	0.266	0.079	1.074

The volume of the equivalent sphere can be calculated by Eq. (7):

$$V_f = \frac{4\pi}{3}\gamma^3 \tag{7}$$

Further, the fractional free volume (*FFV*) may be estimated from Eq. (8):

$$FFV = V_{f3}I_3 \tag{8}$$

where V_f and I are free volume of the sphere and intensity of o-Ps, respectively. The free volume parameters of the as-prepared membranes tabulated in Table 2 indicated that pure CS membrane (Entry 1) possessed free volume cavities with an average radius about 0.276 nm, which was in agreement with the results in the literature [25,53]. The free volume cavity size of hybrid membranes (Entries 2–6) implied the important subtle influence of interfacial interaction on the interface morphology. According to the results of r_3 in Table 2, it is reasonably proposed three possible models of interface morphology as illustrated in Scheme 2. Case I represented the interface morphology of CS/silica-QPy membrane. In this case, the addition of the fillers reduced the hydrogen-bonding interactions between CS chains and simultaneously caused strong and extensive electrostatic repulsive force with CS chains, which synergistically disrupted the ordered chain packing and loosened the chains. Accordingly, the network pores of CS chains became larger (Entry 4, 0.282 nm). Case II corresponded to the situation of CS/silica (Entry 2) and CS/silica-Py (Entry 3) membranes, which possessed a little smaller cavity than pure CS membrane due to the hydrogen-bonding interactions between CS and particles. These interactions would inhibit the CS chains mobility and enhance the stressed at the interface, and thus caused rigidification of CS chains near the filler surface [4,56]. Case III represented the interface morphologies of CS/silica-CO_2H (Entry 5) and CS/silica-SO_3H (Entry 6) membrane. In this case, the formation of strong and extensive electrostatic attractive force would generate strong stress at the organic–inorganic interface during solvent evaporation, which remarkably inhibited the mobility of CS chains and led to dense chain packing, and thus resulted in significant rigidification near the interfacial region. The results of free volume characteristics were well in agreement with the characterization by FITR, XRD and TGA. In summary, the free volume characteristics of the membrane were strongly dependent on the interfacial interaction between the fillers and polymer matrix. Therefore, the morphology (free volume) of the membrane could be tailored by manipulating the interfacial interaction, thus controlled the transport property of the hybrid membrane.

3.4.2. Water uptake, swelling, and methanol permeability

The values of water uptake, swelling and methanol permeability for the test membranes were tabulated in Table 3. It was known that the adsorbed water molecules mainly located near the hydrophilic groups of polymer chains and were accommodated in the free volume cavities [28,35]. The inorganic particles were dense and non-water uptake, so that only the polymeric phase contributed to water uptake, leading to a lower water uptake of the hybrid membranes per mass (45.3–54.5% of water uptake for the hybrid membranes comparing to 68.0% for pure CS membrane). By comparison of the results of water uptake (Table 3) and *FFV* (Table 2), it could be seen clearly that the water uptake increased (from 45.3% for CS/silica-SO_3H to 54.5% for CS/silica-QPy) with increasing *FFV* (from 1.074% to 1.267%) of the membrane. These results verified the strong determination of the water uptake upon the free volume of membrane. The swelling of the membranes caused by the adsorption of water was quite consistent with the result of water uptake. In other words, the high swelling degree of the membranes was obtained via a high water uptake.

The free volume cavities could provide diffusing molecules with a low-resistance path for transport. Penetrant-transporting through a dense membrane is mainly determined by diffusing in the free volume cavities, thus the larger and more numerous free volume elements are, the faster molecules migrate through a membrane [25,54]. Since the average free volume cavity radius (about 0.27 nm) was larger than the kinetic radius of methanol molecule (0.19 nm), methanol transporting through the membrane would occur in free volume cavities. As shown in Table 3, the hybrid membranes displayed much lower methanol crossover than pure CS membrane. Such result was reasonably attributed to the enhancing diffusion resistance, which was caused by the non-permeable particles obstructing the methanol transport and hence lengthened the diffusion pathway [5,15]. Furthermore, the methanol permeability of hybrid membranes (methanol permeability parameter in Table 3) also verified the correlation between free volume characteristics (*FFV* parameter in Table 2) and transport properties of the membranes. In case I, the addition of silica-QPy increased the free volume cavities, and resulted in a high methanol crossover (Entry 5, 1.14×10^{-6} cm^2 s^{-1} in 2 M methanol). Case II behavior manifested itself as methanol permeability (Entry 3 and 4, around 1.05×10^{-6} cm^2 s^{-1}) lower than neat CS membrane, since the membrane formed rigidification at the interface. Case III resulted in lowest methanol crossover (Entries 6 and 7, around 6.45×10^{-7} cm^2 s^{-1}) due to the strong attractive force, which significantly decreased the free volume cavities. The methanol crossover in 12 M methanol solution displayed the same changing trend as that in 2 M methanol solution, which gradually decreased (from 5.54×10^{-7} cm^2 s^{-1} for CS/silica-QPy to 3.77×10^{-7} cm^2 s^{-1} for CS/silica-SO_3H) with reducing *FFV* (from 1.267% to 1.074%) of the membranes. Besides, the methanol permeability was lower (around 50%) in 12 M methanol solution than that in 2 M methanol solution of the membrane. Such phenomenon was reasonably attributed to the properties of aqueous methanol solution and the microstructure of the CS-based membrane, which were elucidated in detail in our previous study [9]. The methanol permeability test clearly revealed a strong dependence of methanol transport upon the free volume characteristics of CS-based membrane.

Nafion 117 (Entry 1), used as reference, was also measured under the same measuring conditions. As could be clearly observed, the CS-based membrane performed much lower methanol crossover than Nafion 117. In particular, CS/silica-CO_2H membrane displayed desirably low methanol crossover, which was only one-fifth (6.60×10^{-7} vs. 31.4×10^{-7} cm^2 s^{-1}) and one-tenth (3.95×10^{-7} vs. 40.1×10^{-7} cm^2 s^{-1}) of that of Nafion 117 in 2 M and 12 M aqueous methanol solution, respectively.

3.5. The proton acceptor/donor capability analysis and proton conductivity evaluation of the membrane

The *IEC* values and proton conductivity of the test membranes were listed in Table 4. According to Table 1, the *IEC* values of the silica and silica–polymer particles varied with the surface groups and followed the order of silica-SO_3H > silica-CO_2H > silica-Py > silica-QPy. The *IEC* values of the membranes shown in Table 4 varied with the ion exchange capacity of the fillers and followed the same trend.

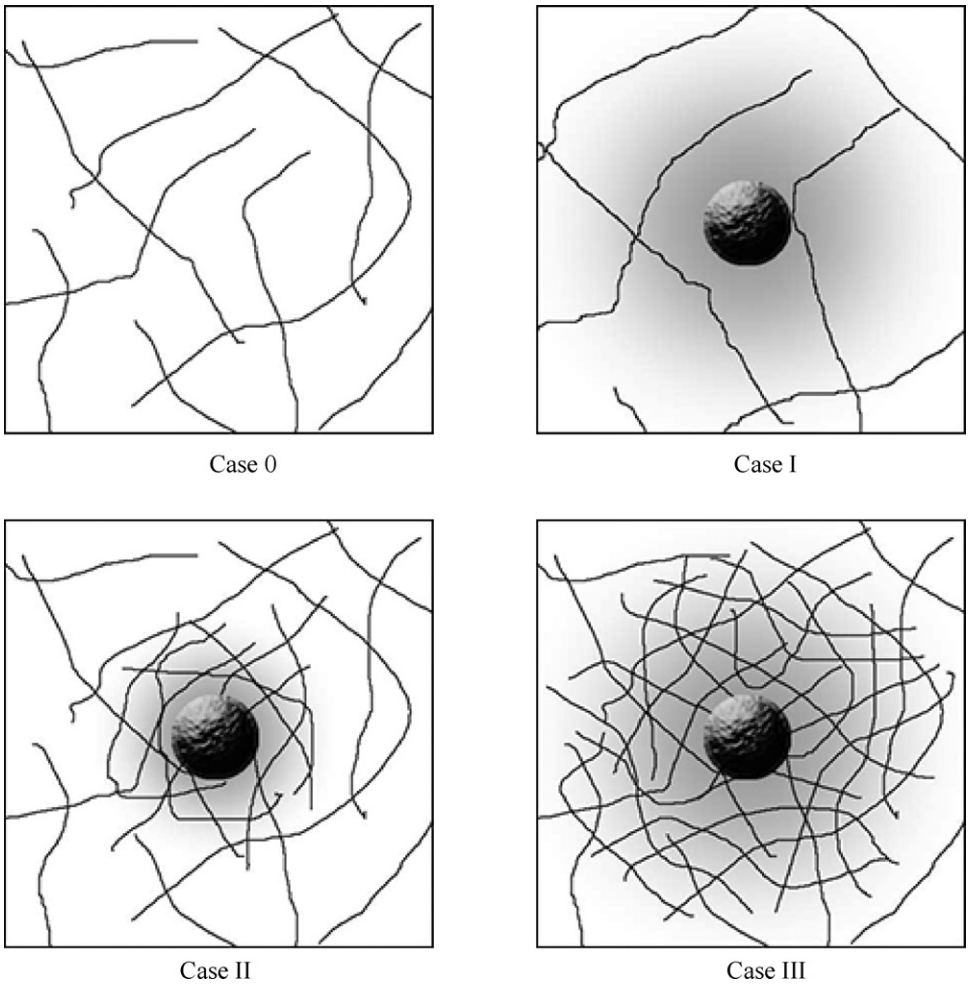

Scheme 2. Schematic illustration of the nanoscale morphologies at the polymer/particle interface. Case 0: morphology of pure CS; Case I: morphology of CS/silica-QPy; Case II: morphology of CS/silica-Py and CS/silica; Case III: morphology of CS/silica-CO_2H and CS/silica-SO_3H.

Table 3
Water uptake, swelling, and methanol permeability of Nafion 117, CS, and hybrid membranes.

Entry	Membrane	Water uptake (%)	Swelling (%)	Methanol permeability (10^{-7} cm^2 s^{-1})	
				2 M methanol	12 M methanol
1	Nafion 117			31.4	40.1
2	CS	68.0	41.6	17.8	8.70
3	CS/silica	53.8	38.5	10.9	5. 37
4	CS/silica-Py	53.4	38.1	10.4	5.25
5	CS/silica-QPy	54.5	38.8	11.4	5.54
6	CS/silica-CO_2H	48.0	35.3	6.60	3.95
7	CS/silica-SO_3H	45.3	33.7	6.31	3.77

Proton migration in polymer electrolyte membrane is well studied and discussed in the view of a vehicle mechanism (protons diffuse accompanying water molecules) and a Grotthuss mechanism (protons hop from one site to a neighboring one), which both exist in CS-based membranes [48,52]. According to Table 4, the proton conductivity decreased (from 0.021 to 0.016 S cm^{-1}) with the incorporation of silica particles (Entry 3) due to the presence of the less-conductive particles, which lengthened the transport pathway and increased the conductive resistance [57]. On the other hand, additional reorganization of the proton environment, consisting of reorientation of individual species or even more extended ensembles, would form an uninterrupted trajectory for proton migration [58]. Therefore, after appropriate chemical modification of the silica surface, the functional groups and adsorbed

Table 4
IEC values and proton conductivity of pure CS and hybrid membranes.

Entry	1	2	3	4	5	6	7
Membrane	Nafion 117	CS	CS/silica	CS/silica-Py	CS/silica-QPy	CS/silica-CO_2H	CS/silica-SO_3H
IEC (mmol g^{-1})	0.886	0.289	0.206	0.272	0.254	0.334	0.493
Proton conductivity (S cm^{-1})	0.069	0.021	0.016	0.019	0.018	0.029	0.024

water would facilitate the proton transport capability (Entries 4–7) according to Grotthuss mechanism, originating from the generation of a continuous proton conductive pathway [5,17,58]. Under this mechanism, the proton acceptor/donor capability of the membrane may determine the proton migration [42]. Compared with the *IEC* value and proton conductivity (Table 4) of hybrid membranes, an interesting phenomenon could be found: the *IEC* values followed the order of CS/silica-SO_3H > CS/silica-CO_2H > CS/silica-Py; however, the proton conductivity was under the order of CS/silica-CO_2H > CS/silica-SO_3H > CS/silica-Py. It was reasonably postulated that: (1) the surface pyridyl group of silica-Py was of basicity, which displayed strong proton acceptor capability but weak donor capability, and the mobile protons might be "trapped" by reacting with basic groups [20]; (2) the —SO_3H groups in CS/silica-SO_3H could dissociate and deliver proton easily, but was difficult to accept proton, as a result the proton would have a strong coulomb resistance when jumping [59]; (3) —CO_2H group was a moderate acid, which possessed moderate proton acceptor capability as well as donor capability, and the acceptor and donor capabilities were well matched. Hence, the energy barrier for proton transport from one carrier to another was low [41,42]. In summary, the results indicated that the membrane should possess matchable proton acceptor/donor capability to facilitate the proton migration.

It is deserved to highlight that the addition of silica-CO_2H significantly increased the proton conductivity by 40% in comparison with pure CS membrane. Although the proton conductivity (Entry 6, 0.029 S cm^{-1}) of CS/silica-CO_2H membrane was a little lower than that of Nafion 117 (Entry 1, 0.0691 S cm^{-1}), it should be still high enough (>0.01 S cm^{-1}) to serve as the proton exchange membranes for DMFC applications [60].

4. Conclusion

Organic–inorganic hybrid membranes were prepared by embedding silica and silica–polymer submicrospheres bearing different functionalizing groups as agents into CS matrix. Manipulating the interfacial (polymer/particle and particle/particle) interaction could tune the dispersion of the submicrospheres within hybrid membranes. The repulsive interaction rendered homogenous dispersion whereas the attractive interaction caused undesirable agglomeration. The incorporation of inorganic particles with different functional groups displayed the dual roles in enhancing the membrane performance: (1) optimizing the interface morphology, which was reflected by the free volume characteristics, through the interaction at the polymer/particle interface. The attractive force led to the reduced free volume cavity size and hence the increased methanol resistance. (2) Constructing the appropriate proton conductive pathway through adjusting the proton acceptor/donor capability. The membranes containing the inorganic particles with most matchable proton acceptor/donor capability exhibited the highest proton conductivity. These findings were confirmed by the results that the incorporation of silica-CO_2H simultaneously reduced the methanol crossover by 63% and increased the proton conductivity by 40% in comparison with pure CS membrane. In summary, it was reasonable to conclude that the high performance of hybrid PEM could be acquired by embedding the appropriately functionalized inorganic fillers to tune free volume characteristics and proton acceptor/donor capability.

Acknowledgements

The authors gratefully acknowledge financial support from the National Nature Science Foundation of China (No.: 20776101), the Programme of Introducing Talents of Discipline to Universities (No.: B06006) and the Cross-Century Talent Raising Program of Ministry of Education of China. We thank Professor Yuxin Wang for his help in the proton conductivity measurements.

References

[1] K.J. Shea, D.A. Loy, Chem. Mater. 13 (2001) 3306–3319.
[2] H.K. Jeong, W. Krych, H. Ramanan, S. Nair, E. Marand, M. Tsapatsis, Chem. Mater. 16 (2004) 3838–3845.
[3] T.C. Merkel, Z. He, I. Pinnau, B.D. Freeman, P. Meakin, A.J. Hill, Macromolecules 36 (2003) 6844–6855.
[4] T.S. Chung, L.Y. Jiang, Y. Li, S. Kulprathipanja, Prog. Polym. Sci. 32 (2007) 483–507.
[5] D.S. Kim, B. Liu, M.D. Guiver, Polymer 47 (2006) 7871–7880.
[6] Q. Li, R. He, J.O. Jensen, N.J. Bjerrum, Chem. Mater. 15 (2003) 4896–4905.
[7] P. Choi, N.H. Jalani, R. Datta, J. Electrochem. Soc. 152 (2005) A1548–A1554.
[8] M. Watanabe, H. Uchida, M. Emori, J. Phys. Chem. B 102 (1998) 3129–3137.
[9] J. Wang, X. Zheng, H. Wu, B. Zheng, Z. Jiang, X. Hao, B. Wang, J. Power Sources 178 (2008) 9–19.
[10] Z. Chen, B. Holmberg, W. Li, X. Wang, W. Deng, R. Munoz, Y. Yan, Chem. Mater. 18 (2006) 5669–5675.
[11] C. Yang, S. Srinivasan, A.B. Bocarsly, S. Tulyani, J.B. Benziger, J. Membr. Sci. 237 (2004) 145–161.
[12] R.F. Silva, S. Passerini, A. Pozio, Electrochim. Acta 50 (2005) 2639–2645.
[13] V. Tricoli, F. Nannetti, Electrochim. Acta 48 (2003) 2625–2633.
[14] S.P. Jiang, Z. Liu, Z.Q. Tian, Adv. Mater. 18 (2006) 1068–1072.
[15] B. Libby, W.H. Smyrl, E.L. Cussler, AIChE J. 49 (2003) 991–1001.
[16] V.S. Silva, B. Ruffmann, H. Silva, Y.A. Gallego, A. Mendes, L.M. Madeira, S.P. Nunes, J. Power Sources 140 (2005) 34–40.
[17] Y.H. Su, Y.L. Liu, Y.M. Sun, J.Y. Lai, D.M. Wang, Y. Gao, B. Liu, M.D. Guiver, J. Membr. Sci. 296 (2007) 21–28.
[18] S.H. Joo, C. Pak, E.A. Kim, Y.H. Lee, H. Chang, D. Seung, Y.S. Choi, J.B. Park, T.K. Kim, J. Power Sources 180 (2008) 63–70.
[19] C.H. Rhee, H.K. Kim, H. Chang, J.S. Lee, Chem. Mater. 17 (2005) 1691–1697.
[20] X. Li, E.P.L. Roberts, S.M. Holmes, V. Zholobenko, Solid State Ion 178 (2007) 1248–1255.
[21] K.D. Sitter, P. Winberg, J. D'Haen, C. Dotremont, R. Leysen, J.A. Martens, S. Mullens, F.H.J. Maurer, F.J. Ivo, Vankelecom, J. Membr. Sci. 278 (2006) 83–91.
[22] Z.X. Liang, T.S. Zhao, J. Prabhuram, J. Membr. Sci. 283 (2006) 219–224.
[23] N. Miyake, J.S. Wainright, R.F. Savinell, J. Electrochem. Soc. 148 (2001) A905–A909.
[24] F. Peng, L. Lu, H. Sun, Y. Wang, J. Liu, Z. Jiang, Chem. Mater. 17 (2005) 6790–6796.
[25] P. Winberg, K. DeSitter, C. Dotremont, S. Mullens, I.F.J. Vankelecom, F.H.J. Maurer, Macromolecules 38 (2005) 3776–3782.
[26] T.C. Merkel, B.D. Freeman, Z. He, I. Pinnau, P. Meakin, A.J. Hill, Chem. Mater. 15 (2003) 109–123.
[27] V.S. Silva, J. Schirmer, R. Reissner, B. Ruffmann, H. Silva, A. Mendes, L.M. Madeira, S.P. Nunes, J. Power Sources 140 (2005) 41–49.
[28] R.Q. Fu, J.J. Woo, S.J. Seo, J.S. Lee, S.H. Moon, J. Power Sources 179 (2008) 458–466.
[29] B.P. Tripathi, A. Saxena, V.K. Shahi, J. Membr. Sci. 318 (2008) 288–297.
[30] Q.F. Li, H.A. Hjuler, N.J. Bjerrum, J. Appl. Electrochem. 31 (2001) 773–779.
[31] G.L. Athens, Y. Ein-Eli, B.F. Chmelka, Adv. Mater. 19 (2007) 2580–2587.
[32] M.A. Hickner, H. Ghassemi, Y.S. Kim, B.R. Einsla, J.E. McGrath, Chem. Rev. 104 (2004) 4587–4612.
[33] J.A. Kerres, J. Membr. Sci. 185 (2001) 3–27.
[34] C.H. Lee, H.B. Park, Y.S. Chung, Y.M. Lee, B.D. Freeman, Macromolecules 39 (2006) 755–764.
[35] S. Zhong, X. Cui, H. Cai, T. Fu, K. Shao, H. Na, J. Power Sources 168 (2007) 154–161.
[36] S.J. Paddison, K.D. Kreuer, J. Maier, Phys. Chem. Chem. Phys. 8 (2006) 4530–4542.
[37] H.R. Allcock, M.A. Hofmann, C.M. Ambler, S.N. Lvov, X.Y. Zhou, E. Chalkova, J. Weston, J. Membr. Sci. 201 (2002) 47–54.
[38] Y.F. Lin, C.Y. Yen, C.H. Hung, Y.H. Hsiao, C.C.M. Ma, J. Power Sources 168 (2007) 162–166.
[39] R.H. He, Q.F. Li, G. Xiao, N.J. Bjerrum, J. Membr. Sci. 226 (2003) 169–184.
[40] J.D. Kim, T. Mori, I. Honma, J. Electrochem. Soc. 153 (2006) A508–A514.
[41] S.R. Narayanan, S.P. Yen, L. Liu, S.G. Greenbaum, J. Phys. Chem. B 110 (2006) 3942–3948.
[42] M. Schuster, T. Rager, A. Noda, K.D. Kreuer, J. Maier, Fuel Cells 5 (2005) 355–365.
[43] K.D. Kreuer, S.J. Paddison, E. Spohr, M. Schuster, Chem. Rev. 104 (2004) 4637–4678.
[44] G. Liu, H. Zhang, X. Yang, Y. Wang, Polymer 48 (2007) 5896–5904.
[45] M. Yang, J. Ma, C. Zhang, Z. Yang, Y. Lu, Angew. Chem. Int. Ed. 44 (2005) 6727–6730.
[46] F. Bai, X. Yang, R. Li, B. Huang, W. Huang, Polymer 47 (2006) 5775–5784.
[47] J. Wang, X. Yang, Langmuir 24 (2008) 3358–3364.
[48] B. Smitha, S. Sridhar, A.A. Khan, Macromolecules 37 (2004) 2233–2239.
[49] J. Wang, X. Yang, Colloid Polym. Sci. 286 (2008) 283–291.
[50] M. Jia, K.V. Peinemann, R.D. Behling, J. Membr. Sci. 73 (1992) 119–128.
[51] V.G. Levich, V.S. Krylov, Annu. Rev. Fluid Mech. 1 (1969) 293–316.
[52] J.R. Salgado, Electrochim. Acta 52 (2007) 3766–3778.
[53] W. Yuan, W. Hong, Z. Bin, Z. Hong, Z. Jiang, X. Hao, B. Wang, J. Power Sources 172 (2007) 604–612.
[54] F. Peng, L. Lu, H. Sun, Y. Wang, H. Wu, Z. Jiang, J. Membr. Sci. 275 (2006) 97–104.

[55] M. García, J. Barsema, R.E. Galindo, D. Cangialosi, J. Garcia-Turiel, W.E. van Zyl, H. Verweij, D.H.A. Blank, Polym. Eng. Sci. 44 (2004) 1240–1246.
[56] T.T. Moore, W.J. Koros, J. Mol. Struct. 739 (2005) 87–98.
[57] F. Pereira, K. Valle, P. Belleville, A. Morin, S. Lambert, C. Sanchez, Chem. Mater. 20 (2008) 1710–1718.
[58] K.D. Kreuer, Chem. Mater. 8 (1996) 610–641.
[59] E. Spohr, P. Commer, A.A. Kornyshev, J. Phys. Chem. B 106 (2002) 10560–10569.
[60] V. Neburchilov, J. Martin, H. Wang, J. Zhang, J. Power Sources 169 (2007) 221–238.